ELSEVIER

Chemical Engineering Journal 123 (2006) 71–80

Chemical Engineering Journal

www.elsevier.com/locate/cej

# Mechanism and prediction of bed agglomeration during fluidized bed combustion of a biomass fuel: Effect of the reactor scale

Riccardo Chirone, Francesco Miccio, Fabrizio Scala *

*Istituto di Ricerche sulla Combustione-CNR, P. le Tecchio 80, 80125 Napoli, Italy*

Received 27 January 2006; received in revised form 4 July 2006; accepted 12 July 2006

**Abstract**

The fluidized bed combustion of a biomass residue (pine seed shells) was investigated both in a bench-scale and in a pilot-scale reactor. Extensive bed agglomeration problems were experienced during combustion of this fuel, as a consequence of the high content of alkali species in the ash. The focus of the study was the effect of the combustor scale and of the operating conditions on the characteristic time and the extent of bed agglomeration during combustion. Bed defluidization times as well as the extent of ash accumulation in the bed were measured at different operating conditions in the two reactors. Results indicated that sand size, combustor size, and presence of internals had a significant influence on the agglomeration phenomenon. SEM/EDX analysis on agglomerate samples discharged from the bed after defluidization confirmed that bed agglomeration is a consequence of potassium and sodium enrichment on the sand particle surface, in conjunction with high temperature spots near burning char particles. The competition between formation of stable bonds between bed particles and the breaking of the agglomerates by inertial forces is the key mechanism leading to bed agglomeration. In addition, a previously developed diagnostic tool based on the measurement of the dynamic pressure signal inside the bed was successfully tested with the present biomass fuel and at both combustor scales for its capability to predict the bed defluidization onset.


*Keywords:* Fluidized bed combustion; Bed agglomeration; Biomass; Alkali; Pine seed shells

## 1. Introduction

Fluidized bed combustion (FBC) is awarded as an effective technology for burning both conventional and renewable solid fuels [1,2]. The flexibility toward the fuel, the high combustion efficiency, and the low environmental impact are the major advantages of FBC. However, during combustion of biomass fuels a number of operational problems can be experienced, mainly related to the combustion of volatile matter [3,4] and to the fate of the ash components [5–7]. The formation of particle agglomerates in the bed is one of the most likely phenomena occurring during biomass combustion. This unwanted process, in the absence of counter-measures, leads to the whole bed agglomeration and consequent defluidization [5–8]. Therefore, preventing bed agglomeration is a relevant task to avoid unscheduled shutdowns and costly maintenance stops for the boiler.

The onset of bed agglomeration is mostly attributed to the presence of alkali species in the ash of biomass fuels (sodium and potassium). The interaction between alkalis and silica sand under high temperature conditions leads to the formation of low-melting point eutectics on the surface of the bed particles [9]. Under prolonged operation this sticky superficial layer leads to the formation of permanent bonds between sand particles, representing the early stage of the agglomeration process. A further stimulus for bed agglomeration can be found in the local temperature rise associated to the combustion of both fine and coarse char particles. Thanks to the high reactivity of the biomass char, the abraded fine particles could be effectively burnt inside the bed. They could give rise to hot spots on the surface of sand particles, where the ash undergoes softening, melting, and vaporization, even at relatively low bed temperatures [10–13]. Despite a considerable research effort has been devoted to this subject [14–17], the detailed mechanisms of ash–bed material interaction and of bed agglomeration are not well understood yet. Recently, a thorough review of the proposed mechanisms for bed agglomeration during biomass fuels FBC was reported [18]. Based on experimental data available in the literature and

* Corresponding author. Tel.: +39 081 7682969; fax: +39 081 5936936.
*E-mail address:* scala@irc.na.cnr.it (F. Scala).

1385-8947/$ – see front matter © 2006 Elsevier B.V. All rights reserved.
doi:10.1016/j.cej.2006.07.004

**Nomenclature**

| | |
|---|---|
| $C_K$ | potassium concentration |
| $d_b$ | bed particle size |
| $e$ | excess air factor |
| $P$ | pressure |
| $t$ | time |
| $T$ | bed temperature |
| $U$ | fluidization velocity |
| $W_{ash}$ | percent of accumulated ash in the bed at agglomeration |
| $W_b$ | bed inventory |
| $z$ | elevation |

*Greek letters*

| | |
|---|---|
| $\eta$ | combustion efficiency |
| $\sigma_P^2$ | pressure variance |
| $\tau$ | defluidization time |
| $\Psi$ | ratio between potassium added with fuel and bed mass |

on their own results, the authors concluded that the most likely alkali species transfer mechanism relies on collisions of sand with burning char particles. The authors further suggested that bed agglomerates start to form near burning char, where the higher temperatures enhance the formation of melt and, in turn, the particles stickiness.

The formation of particle aggregates strongly affects pressure and temperature signals of bed sensors. Large fluctuations in pressure and temperature were experienced during agglomeration experiments with the combustion of coal under reducing conditions [19]. Similarly, unstable profiles of temperature and pressure during the combustion of a biomass (olive husk) were reported in the time interval before agglomeration [18]. It was also noted that in correspondence of the perturbation of the temperature and pressure signals, the variance of the pressure exhibited a well marked decrease [18]. These results were interpreted as a change of fluid-dynamic conditions in the bed, reflecting a less uniform mixing behaviour, and possibly indicating a faster accumulation of ashes in the bed. Repeated tests at bench scale proved that a 60–70% decrease in the pressure variance was typically associated to the agglomeration onset.

The present study provides further insights to understanding the complex pathway to bed agglomeration. An experimental campaign was carried out with two experimental facilities of different scale by burning a biomass fuel (pine seed shells) to systematically achieve bed agglomeration. The research sheds light upon the effect of the combustor size on the characteristic time and the extent of bed agglomeration, the accumulation rate of ash alkalis in the bed, and the mechanism by which the agglomeration takes place. In addition, the previously proposed diagnostic tool based on the measurement of the dynamic pressure signal inside the bed [18] was tested for its ability to predict the bed agglomeration onset both with a different biomass fuel and at a more large and significant combustor scale.

## 2. Experimental

Steady state combustion tests were performed under atmospheric conditions in two bubbling fluidised bed facilities of different scale.

### 2.1. Lab-scale facility

The experimental apparatus FBR102, sketched in Fig. 1, consisted in a cylindrical fluidized bed, a set of pressure transducers and thermocouples, a fuel feeding system, a gas analysis system and a data acquisition unit. The reactor was made by a stainless steel tube with a inner diameter of 102 mm and a height of 1.625 m. The vessel was fitted with a stainless steel perforated distributor plate with 518 holes 0.5 mm in diameter disposed in triangular pitch. The wind-box was packed with ceramic rings to act as gas pre-heater. The distributor and the wind-box packing attained uniform fluidizing gas feeding into the fluidized bed. The vessel was equipped with five sockets (1/2 in. tubes) wall mounted at different heights. The tube located at height $z = 95$ mm was used for fuel feeding, those located at $z = 45$, 145, 245 mm were fitted with a pressure tap and a thermocouple, while the tube located at $z = 775$ mm was fitted only with a thermocouple.

The flue gas exiting the combustor was directed to a high efficiency cyclone for fine particles collection. After the cyclone the flue gas was sampled for gas analysis. A paramagnetic analyzer and two NDIR analyzers were used for on-line measurement of $O_2$, CO and $CO_2$ concentrations, respectively, in the exhaust gases.

The combustor was electrically heated by means of ceramic heaters. The reactor temperature was controlled by two PID con-

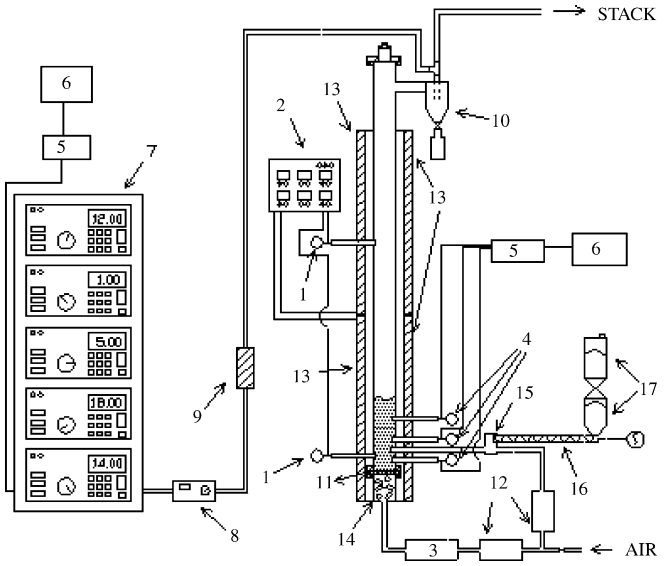


Fig. 1. Bench-scale apparatus (FBR102): (1) thermocouple; (2) temperature PID controller; (3) pre-heater; (4) thermocouple and pressure transducer; (5) acquisition data unit; (6) personal computer; (7) gas analyzers; (8) condenser; (9) filter; (10) cyclone; (11) gas distributor; (12) mass flow controller; (13) ceramic heaters; (14) windbox; (15) fuel–air mixer; (16) screw feeder; (17) fuel hopper.

trollers driven by the signal from the thermocouples inserted nearby the column wall by means of the tubes located at $z$ equal to 45 and 775 mm. The fluidizing gas was preheated to 500 °C in an electrical heater. The fluidization column was equipped with an air-assisted solids metering/feeding system for continuous injection of the fuel at the bottom of the bed. The feeding system consists of a fuel hopper mounted over a screw feeder that further delivers the particles in a mixing chamber where a swirled air stream pneumatically conveys the fuel within the bed. Fluidizing and fuel feeding air streams were metered with two mass flow controllers.

The column was equipped with three high-precision piezoresistive electronic pressure transducers, characterized by a high temporal resolution. These transducers were used to measure the gas pressure profile along the fluidized bed height. The acquisition data unit consisted of a personal computer equipped with a 16 A/D data acquisition board characterized by a high sampling rate. The acquisition data unit was used for measuring gas concentration, temperature and pressure signals at a sampling frequency of 100 Hz.

### 2.2. Pilot-scale facility

The pilot-scale FBC370 facility is sketched in Fig. 2. The AISI 310 stainless steel fluidization column had a circular section (370 mm i.d.) and a total height of 4.65 m. The lower section of the column contained the plenum chamber and the pipe-type distributor equipped with 55 vertical tuyeres. The distributor sustained the bed material allocated in the intermediate section,

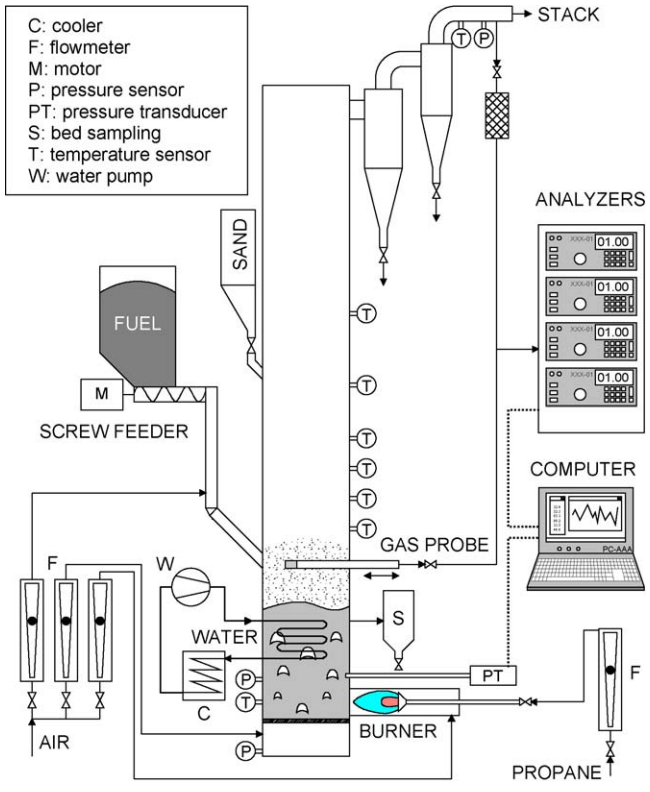


Fig. 2. Pilot-scale apparatus (FBC370).

where several access ports were available. The heat exchange was accomplished by an array of horizontal bayonet-type tubes whose adjustable penetration into the bed controlled the heat removal rate. The higher section of the fluidization column (freeboard) was also fitted with several ports for temperature, pressure and gas concentration probes. Two cyclones, the first with medium and the second with high efficiency, were used for capturing the fly ash. Thermal insulation with a ceramic blanket minimises heat losses from the vessel.

FBC370 was equipped with a continuous over-bed feeding system. Fuel particles were fed by means of a screw-type metering device and were dropped on bed surface after the passage throughout an inclined tube at $z = 941$ mm.

Piezoresistive pressure transducers with a high sampling rate (>1000 Hz) were used to measure the gas pressure profile along the fluidized bed height. The pressure signals were acquired at a frequency of 100 Hz by means of a personal computer equipped with a 16 bit A/D data acquisition board and a specifically developed software for the elaboration of the measurements in real time.

### 2.3. Materials

Quartz sand with the two nominal sizes 0.300 and 0.725 mm were used as bed inert material for both the bench-scale and the pilot-scale combustor. The bed inventory was 3.3 kg in the bench-scale facility and 60 or, alternatively, 85 kg in the pilot-scale combustor.

A biomass fuel, shells of pine seeds (*Pinus pinea*), was used for all experimental tests. The fuel particles have in origin an irregular and drop like shape (approximately 30 mm × 10 mm in size), high mechanical resistance and anisotropic properties. In order to ensure a reliable fuel feeding, pine seed shells were crushed and sieved; the size ranges adopted were 1.0–3.3 and 1.0–6.3 mm for bench-scale and pilot-scale facilities, respectively. Only one pilot-scale test (Run #12, with 0.725 mm sand size) was carried out by feeding the as received uncrushed biomass particles. Table 1 summarizes the properties of the fuel. The biomass can be considered as a typical ligneous, high-volatile, and low-ash fuel. It is worth noting that the total content of K and Na oxides in the ash attains a value as high as ∼17% by mass.

### 2.4. Experimental procedure

The operating conditions for the experiments are summarized in Table 2. The bed temperature was fixed at 850 or 900 °C for all tests. The fluidization velocity was in the ranges 0.5–0.7 and 0.7–1.0 m/s for bench-scale and pilot-scale facility, respectively. The start-up of FBR102 was accomplished by electrically heating the bed of inert sand. When the bed temperature reached a value of 750 °C the fuel feeding was started. The fuel feed was adjusted in the range 0.5–0.7 kg/h to reach the desired excess air value (in the range 30–90%). During the run temperature, pressure and gas concentration data were continuously logged on the PC. Every 15–20 min elutriated material collected at the cyclone was measured and analyzed for carbon concentration, for cal-

Table 1
Properties of pine seed shells

| | |
|---|---|
| Particle density (g/cm$^3$) | 1.2 |
| LHV (kJ/kg) | 15200 |
| Proximate analysis (as received, wt.%) | |
| Moisture | 11.9 |
| Volatiles | 67.5 |
| Fixed carbon | 19.3 |
| Ash | 1.3 |
| Ultimate analysis (dry basis, wt.%) | |
| Carbon | 49.8 |
| Hydrogen | 6.2 |
| Nitrogen | 0.3 |
| Sulfur | <0.1 |
| Ash | 1.5 |
| Oxygen (diff.) | 42.1 |
| Ash composition (wt.%) | |
| CaO | 2.6 |
| MgO | 2.7 |
| $K_2O$ | 15.0 |
| $Na_2O$ | 1.8 |
| $Fe_2O_3$ | 0.4 |
| $Al_2O_3$ | 0.3 |
| $SiO_2$ | 72.9 |
| $P_2O_5$ | 0.6 |
| $SO_3$ | 2.2 |

culation of the unburned carbon flow rate at the exhaust. Mass balance closures on carbon and oxygen were always within 3% error. The run ended when agglomeration of the bed occurred, as indicated by a jump in the temperature and pressure profiles within the bed. The total time interval from the beginning of the fuel feeding to the agglomeration onset was recorded. After the end of the run, the bed was cooled down and discharged from the combustor, weighed and sieved for agglomerates separation.

The FBC370 start-up was accomplished thanks to a propane burner that directly discharged hot gases inside the bed. After the bed reached a temperature high enough to ignite fuel particles (e.g. 700 °C), the feeding of fuel was started and propane was switched off. The fuel feed was adjusted in the range 13–17 kg/h to reach the desired excess air value (in the range 20–30%). Temperatures, pressures and flue gas concentrations ($O_2$, $CO_2$, CO, $CH_4$, $N_2O$ and NO) in the exhausts were on-line monitored and recorded. If the agglomeration was not experienced, the run was quickly interrupted at the end of the working day. In the next day the test was restarted from a warm condition until the agglomeration of the bed occurred. This event was indicated by large fluctuations in temperature, concentration, and pressure profiles, and the ineffectiveness of any control action. The total time interval from the beginning of the fuel feeding till the agglomeration onset was recorded. As bed agglomeration was achieved, the fluidization air was turned off. In a short time, the sand was discharged from the column, weighed and sieved for agglomerates separation.

Selected agglomerate samples from both kinds of tests were observed under a scanning electron microscope (SEM) and subjected to energy dispersive X-ray (EDX) elemental analysis. Few samples were embedded in epoxy resin and then cut and polished for SEM observation and EDX elemental mapping of agglomerate cross-sections.

### 2.5. Quartz sand laboratory characterization

The sand material was subjected to a laboratory characterization aimed at determining the minimum amount of potassium to be added to the fresh sand for achieving agglomeration. A sand sample (5.3 g) was progressively enriched in potassium by adding drops of a solution of KOH in distilled water and treating the wet sample in a muffle furnace at 800 °C. The occurrence of agglomeration was visually checked. Repeated tests showed that the minimum K amount required for agglomeration was 0.012 g/1 g of sand.

## 3. Results and discussion

### 3.1. Comparison between bench-scale and pilot-scale agglomeration experiments

Table 2 reports a summary of the operating conditions and the main results of the experiments carried out in this work in

Table 2
Summary of operating conditions and main results of the pine seed shells combustion experiments

| Run # | Test rig | $W_b$ (kg) | $T$ (°C) | $U$ (m/s) | $e$ (–) | $d_b$ (μm) | $\eta$ (%) | $\tau$ (min) | $W_{ash}$ (%) |
|---|---|---|---|---|---|---|---|---|---|
| 1 | Lab scale | 3.3 | 850 | 0.52 | 1.40 | 212–400 | 96.9 | 320 | 0.95 |
| 2 | Lab scale | 3.3 | 850 | 0.71 | 1.89 | 212–400 | 98.6 | 318 | 1.2 |
| 3 | Lab scale | 3.3 | 850 | 0.55 | 1.35 | 212–400 | 96.9 | 320 | 1.3 |
| 4 | Lab scale | 3.3 | 850 | 0.50 | 1.75 | 212–400 | 97.7 | 388 | 1.1 |
| 5 | Lab scale | 3.3 | 900 | 0.53 | 1.78 | 212–400 | 97.8 | 31 | 0.21 |
| 6 | Lab scale | 3.3 | 900 | 0.52 | 1.23 | 212–400 | 96.8 | 35 | 0.14 |
| 7 | Lab scale | 3.3 | 850 | 0.54 | 1.58 | 600–850 | 97.8 | 702 | 2.3 |
| 8 | Pilot scale | 60 | 850 | 0.74 | 1.26 | 212–400 | 100 | 820 | 2.5 |
| 9[a] | Pilot scale | 60 | 850 | 0.81 | 1.29 | 212–400 | 99.9 | 325 | 1.0/3.3[b] |
| 10[a] | Pilot scale | 60 | 850 | 0.82 | 1.25 | 212–400 | 100 | 133 | 0.51/3.5[b] |
| 11[a] | Pilot scale | 60 | 850 | 0.84 | 1.18 | 212–400 | 99.9 | 56 | 0.22/3.4[b] |
| 12 | Pilot scale | 85 | 850 | 0.99 | 1.26 | 600–850 | 99.9 | 1658 | 7.1 |

[a] In these tests the initial bed inventory was mostly (∼90%) composed of exhausted sand from the previous test.
[b] The first value represents the incremental increase of the ash percentage in the bed at the end of the test; the second value represents the estimated total accumulated ash percentage in the bed at defluidization, assuming an initial bed inventory composed of 90% exhausted sand from the previous test and 10% fresh sand.

the two facilities. The pine seed shells combustion tests were performed at different bed temperatures ($T$), fluidization velocities ($U$), excess air factors ($e$) and inert bed particle sizes ($d_b$). The overall results of the experiments are reported in terms of combustion efficiency ($\eta$), defluidization time ($\tau$), and percent of ash accumulated in the bed at defluidization ($W_{ash}$).

Total combustion efficiencies higher than 96.8% were found for all the experiments carried out in the bench-scale FB, and higher than 99.9% in the pilot-scale FB. It must be underlined that in the bench-scale apparatus volatile species combustion in the freeboard was not optimized, since this work focus on the bed agglomeration behaviour.

All the experiments (in both facilities) eventually ended with bed defluidization. The occurrence of bed agglomeration was clearly detectable from temperature and pressure measurements in the combustor. Upon defluidization, the temperatures in the lower section of the bed tended to peak down, while those in the upper section of the bed peaked up. This trend is consistent with data reported in the literature [8,18] and should be related on the one hand to the decrease of the heat transfer coefficients when the bed is defluidized and on the other hand to the segregated fuel combustion in the upper bed region. In addition, upon defluidization all the pressures within the bed abruptly peaked down because of the onset of bed channeling.

Fig. 3A shows the measured defluidization time ($\tau$) for all the combustion runs in FBR102 and FBC370, as a function of the excess air factor. Defluidization time is defined as the time interval between the start of the fuel feeding and the bed defluidization occurrence. Analysis of data reported in Fig. 3 clearly shows that faster agglomeration occurred with a higher operating temperature. The excess air and the fluidization velocity had a limited influence on the results, at least within the range tested in this work. The temperature effect is consistent with literature data [17,18] reporting that agglomerate formation is enhanced at higher temperatures, where it is easier to reach low-melting point eutectics at the inert particle surface. In the experiments carried out with a larger sand particle size (Runs #7 and 12) the defluidization time approximately doubled with respect to the corresponding experiments where the smaller sand was used (Runs #1 and 8). A possible explanation of this result might rely on the consideration that larger bed particles have more inertia and consequently are associated to more energetic collisions, so that adhesion of the particles to each other to form agglomerates should be more difficult [18]. It clearly appears from analysis of Fig. 3 that the combustor scale exerts a relevant role, the defluidization time being around 2.5 higher in the larger facility under similar operating conditions (Runs #2 and 8). This result can be attributed to the different bed fluid-dynamics and the presence of internals (i.e. the horizontal cooling tubes) in FBC370.

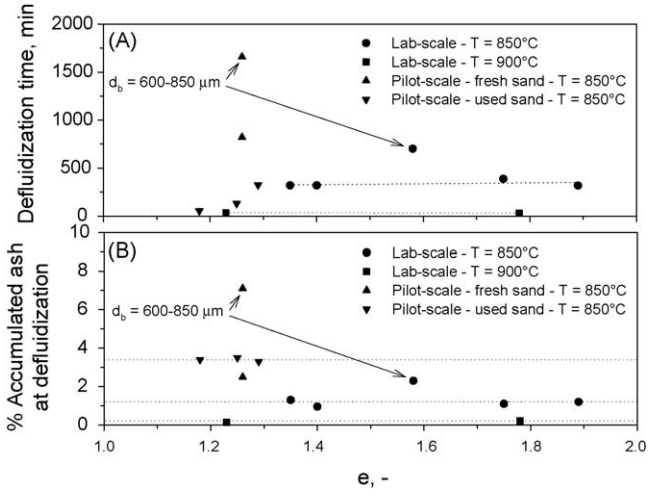


Fig. 3. Defluidization time (A) and weight fraction of ash accumulated in the bed at defluidization (B) as a function of the excess air factor for all combustion experiments ($d_b$ = 212–400 μm).

It must be noted (Table 2) that Runs #9–11 in the pilot-scale facility were carried out by using an initial bed inventory mostly (∼90%) composed of exhausted sand from the previous test, while only ∼10% of the bed weight consisted of fresh sand. Obviously, as a large fraction of the bed material was already enriched in ash, for these runs the defluidization time was substantially shorter than for Run #8, where an initial 100% fresh sand bed was used.

Fig. 3B reports, as a function of the excess air value, the maximum weight fraction of ash accumulated in the bed ($W_{ash}$) at the end of each combustion run. This quantity is calculated as the total ash inlet with the fuel feed during the run divided by the inert bed weight and multiplied by 100. It must be underlined that this is a theoretical quantity as the elutriation loss of both sand and ash during the run is not taken into account in the calculation. Inspection of Fig. 3 shows that irrespective of the excess air value and fluidization velocity, a well-defined ash content was necessary to defluidize the bed, depending on the bed temperature and on the scale of the combustor. In particular, ∼1.2 and ∼0.2% ash contents were calculated for the runs carried out in the bench-scale FB at 850 and 900 °C, respectively, and ∼2.5% ash content for the run carried out in the pilot-scale at 850 °C. Consistently with the defluidization time results, in the experiments carried out with a larger sand particle size the amount of ash necessary to defluidize the bed was larger than that necessary in the corresponding experiment where the smaller sand was used.

For Runs #9–11 in the pilot-scale facility, the maximum weight fraction of ash accumulated in the bed at defluidization was estimated assuming an initial bed inventory composed of 90% exhausted sand from the previous test and 10% fresh sand (Table 2). Noteworthy, a value of ∼3.4% was calculated, which is not much different from the ∼2.5% figure obtained when an initial 100% fresh sand bed was used.

### 3.2. Potassium enrichment in the bed

From now on the focus is devoted to potassium, since this is the major element in the biomass ash responsible for the bed agglomeration. During the experiments, potassium entering the combustor with the fuel feed was steadily accumulated in the bed, so that the relative amount of K requested for bed defluidization ($\Psi$) can be calculated as the ratio between the mass of the added potassium and the bed inventory. $\Psi$ was nearly constant for the bench-scale Runs #1–4 (∼0.13%), and was equal to

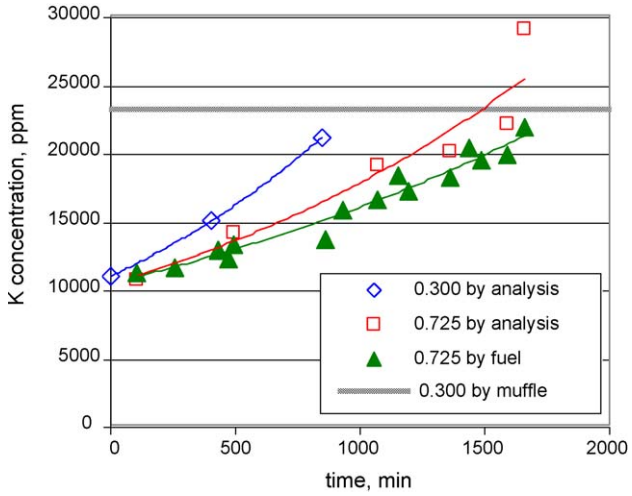


Fig. 4. Potassium concentration in the bed as a function of time during pilot-scale Run #8 ($d_b$ = 0.300 mm) and Run #12 ($d_b$ = 0.725 mm).

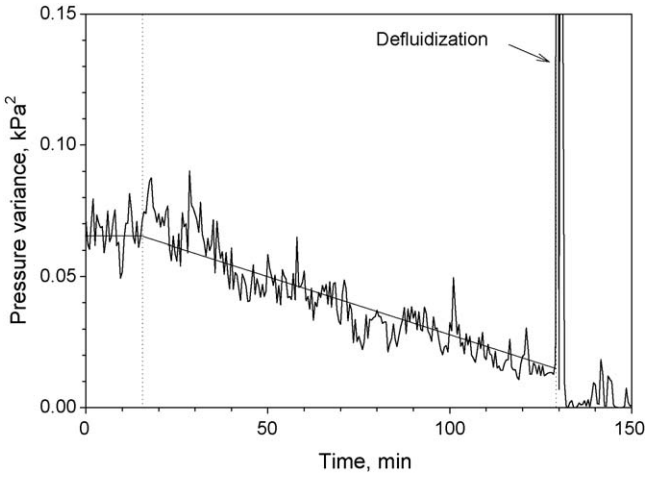


Fig. 5. Gas pressure variance profile at steady state for the bench-scale combustion Run #3. Fuel: pine seed shells; $T$ = 850 °C; $U$ = 0.55 m/s; $e$ = 1.35; $d_b$ = 212–400 μm.

0.47 and 1.13% for pilot-scale Runs #8 and 12, respectively. The enhancement of $\Psi$ of a factor of 3.6 moving from the bench-scale to the pilot-scale facility was reasonably due to the increase of inertial forces that acted inside the bed and contrasted the formation of sand aggregates. This hypothesis is also confirmed by the comparison between Runs #8 and 12. In fact, the potassium requested for defluidization in the latter run was more than doubled, as a consequence of using coarser bed particles and of increasing the fluidization velocity from 0.7 to 1.0 m/s, both changes leading to an enhancement of the inertial forces in the bed.

The actual potassium concentration $C_K$ in bed samples taken from FBC370 at increasing times during Runs #8 and 12 was determined by standard chemical analysis (acid dissolution and mass-spectrometry). The results are reported in Fig. 4 (open symbols) for both experimental tests. In the same figure data points (closed symbols) are also reported for the theoretical value of $C_K$ calculated from the fuel feed rate by assuming that all potassium in the fuel ash is kept in the bed (for Run #12). From the data in Fig. 4 it appears that: (i) potassium is steadily accumulated in the bed during the tests, (ii) there is a rather good agreement between the measured and the calculated K concentration and (iii) the agglomeration occurred as $C_K$ exceeded the threshold values of 21,000 and 25,000 ppm for Runs #8 and 12, respectively. These values are close to the experimental one obtained in the muffle furnace (see Section 2) and reported as a horizontal line at $C_K$ = 23,000 ppm in the same figure. The higher enrichment rate in K noted for Run #8 is an obvious consequence of the lower bed inventory. On the whole, results indicate that the sand is able to effectively capture the fuel potassium, also in the case when a lower bed inventory was used.

### 3.3. Analysis of the pressure variance signal

Figs. 5 and 6 report the pressure variance profiles inside the bed during two runs in bench-scale and pilot-scale facilities, respectively, for a wide time interval before defluidization onset ($t$ = 135 and 115 min). Time zero in the two figures was arbitrarily chosen within the steady state combustion period of the runs. The pressure variance ($\sigma_P^2$) is defined as the average value of the squared difference between the instantaneous measured pressure and the average pressure calculated within a definite time interval (30 and 100 s for bench-scale and pilot-scale tests, respectively): $\sigma_P^2 = \overline{(P - \bar{P})^2}$. In Fig. 5 (bench-scale test) the variance calculated from the pressure signal taken at the middle section of the bed ($z$ = 0.145 m) is shown. This variance was found to be the most regular among those calculated from the three measured pressures [18]. The pressure variance represents the average amplitude of the pressure fluctuations around the average value in the chosen interval and it is linked to the local fluid-dynamic conditions in the measuring bed section. In particular, the pressure variance is affected by phenomena like gas turbulence, and bubbles formation, passage, coalescence, and

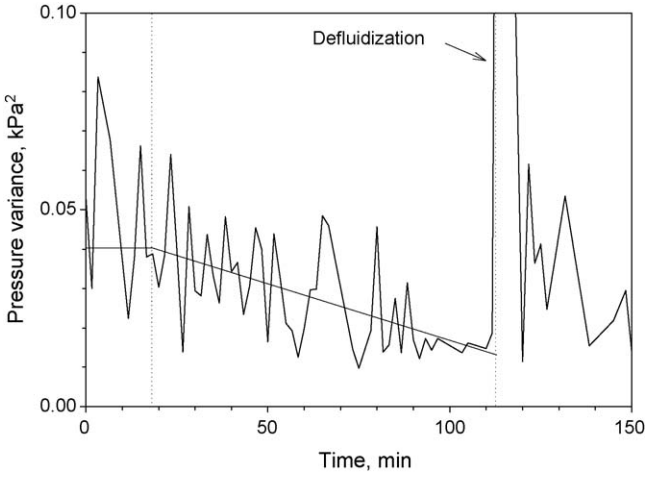


Fig. 6. Gas pressure variance profile at steady state for the pilot-scale combustion Run #9. Fuel: pine seed shells; $T$ = 850 °C; $U$ = 0.81 m/s; $e$ = 1.29; $d_b$ = 212–400 μm.

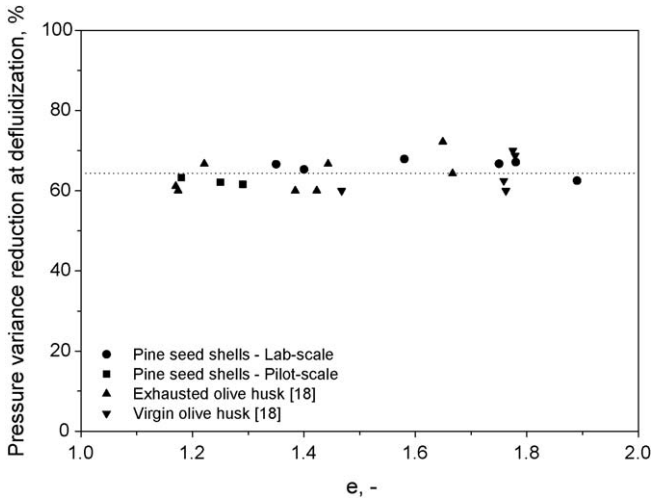


Fig. 7. Gas pressure variance reduction at defluidization as a function of the excess air factor for all combustion experiments carried out in this work and in Ref. [18].

eruption. Fig. 5 shows that while in the first period of the run the variance was approximately constant, in the second period it steadily decreased until bed defluidization. A ∼60% decrease of the variance from the steady average value was measured at the defluidization onset ($t$ = 130 min). This pressure variance decrease might be connected either to an increase of the average size of the bed particles as agglomerates start to form in the bed, or to a change of bed fluid-dynamics due to a decrease of the effectiveness of solids mixing. A similar behaviour of the pressure variance (Fig. 6) was observed during the pilot-scale test until bed defluidization ($t$ = 113 min). The larger fluctuations in the pressure variance in this case must be ascribed to the less controlled conditions of operation (e.g. presence of pressure fluctuations induced by the intermittent operation of the air compressor). Fig. 7 reports the pressure variance reduction upon defluidization with respect to the steady state value for all the combustion runs carried out in this work, as a function of the excess air. In the same figure also results of bench-scale olive husk combustion runs taken from Ref. [18] are reported, for comparison. A fairly constant value of 60–70% was measured for all the runs in both bench-scale and pilot-scale, independently of the operating condition, fuel-type and bed sand size.

On the whole, present results confirm that the pressure variance reduction might be a useful criterion to confidently predict the onset of bed defluidization. In particular, the scale-up of this diagnostic tool was demonstrated by the data obtained in the pilot-scale facility FCB370 (square symbols in Fig. 7). A closer look on Figs. 5 and 6 reveals that the pressure variance was progressively reduced from the initial value to the one obtained just before defluidization conditions occurred in a time scale of the order of hours. This result was verified for all the combustion runs carried out with fresh sand. Therefore, the pressure variance reduction criterion might be applied as a real-time indicator of the formation of agglomerates in the bed, allowing the operator or the automatic control system to adopt well in advance counter-measures to prevent dramatic defluidization events.

### 3.4. Analysis of sand agglomerate samples collected after bed defluidization

At the end of each combustion test the bed was discharged for further characterization. The agglomerates discharged from the reactor appeared to be quite weak and were easy broken into smaller ones. Agglomerates collected after bench-scale tests typically showed a hollow structure, indicating that a burning fuel particle was likely located inside and possibly initiated the agglomeration process. For the tests carried out with the smaller sand size (0.300 mm) the agglomerates showed a maximum size of approximately 5 mm, while when the larger sand size was used (0.725 mm) the maximum agglomerate size was approximately 10 mm. However, the bed discharge procedure is likely to have influenced the particle size distribution of the bed by partly breaking the agglomerates. Two different zones could be observed by SEM analysis within the agglomerates: in the first one the sand particles appear to be completely embedded in a fused layer of material, while in the second one the sand particles are only attached one to the other by fused material necks. The first kind of zone was typically found in the innermost part of the agglomerates, indicating that higher temperatures were experienced inside. An enrichment of potassium and sodium was observed during EDX analysis in both zones, especially in the fused material.

Similar results were obtained after pilot-scale tests carried out with the smaller sand size (0.300 mm). In this case, however, the agglomerates showed a maximum size of approximately 20 mm, larger than that found for the corresponding bench-scale tests. Selected large agglomerate samples were embedded in epoxy resin and then cut and polished for SEM observation and EDX elemental mapping of cross-sections. Fig. 8 shows a SEM micrograph of the cross-section for a typical agglomerate collected after Run #8. The agglomerate appears to be rather loosely packed with sand particles (dark grey) attached together by either layers or necks of fused material (light grey). Fig. 9 reports the window "A" in Fig. 8 observed at a higher magnification under

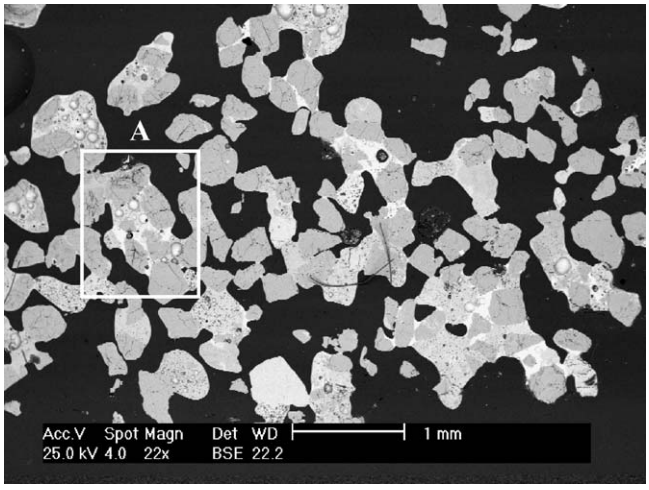


Fig. 8. SEM micrograph of the cross-section of part of a large agglomerate sample from Run #8. Black zones represent epoxy resin in which the sample is embedded.

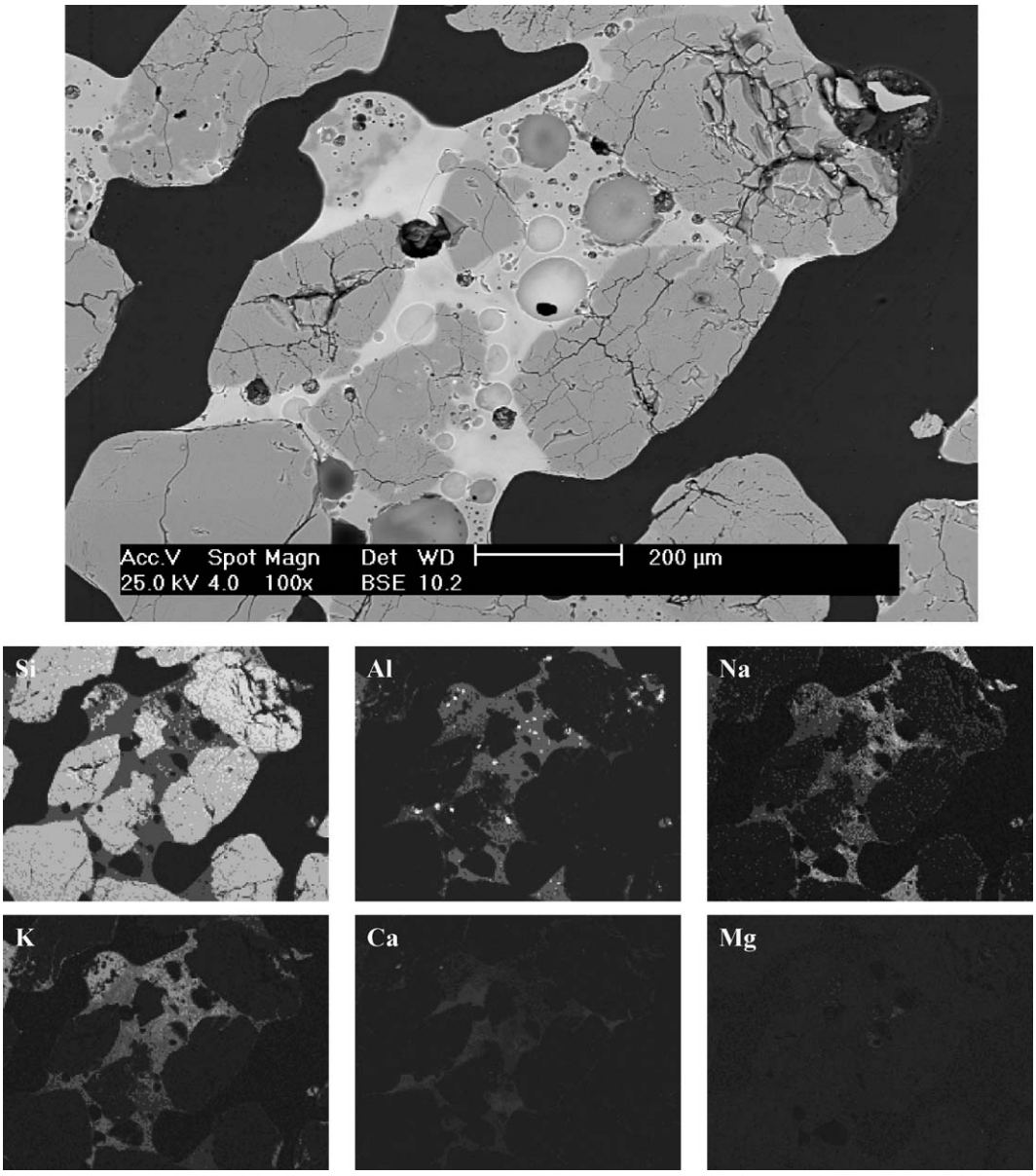


Fig. 9. SEM micrograph and EDX elemental maps of the agglomerate cross-section window "A" in Fig. 8.

the SEM. The figure also reports EDX elemental mappings of selected elements for the cross-section window examined. A lighter area in the maps indicates a higher concentration of the element. It is evident in the figure that a number of sand particles (mainly composed of silica) are embedded in a melt containing silica, potassium and sodium, with lower amounts of calcium, magnesium and aluminium (and Fe and P, not shown in Fig. 9). It must be noted that some aluminium spots appearing in the maps derive from impurities coming from the sample polishing procedure and were not originally present in the agglomerate.

The pilot-scale Run #12 carried out with the larger sand size (0.725 mm) gave rise to a dramatic agglomeration that involved the whole bed inventory, as revealed by the internal inspection of the combustor chamber after the end of the run, where sand adhering to the internal surfaces and large clusters blocked between the horizontal tubes were found. Fig. 10 shows a photograph of a large sand aggregate obtained after Run #12. Similar smaller agglomerates were also discharged from the bed. Inspection of these agglomerates revealed that many cavities were present in the cluster, that were clearly generated upon complete burn-off of entrapped fuel particles after bed agglomeration (Fig. 10).

Another interesting finding arises from the analysis of Fig. 11 that compares an original fuel particle (A), a char particle (B), and a small sand aggregate retrieved from the bed (C) after Run #12. It is worth noting that the aggregate shown in Fig. 11C has comparable size and is similar in shape to the original fuel particle (Fig. 11A). It can be argued that the sand particles stuck on a burning char particle during its conversion and formed a melt with ash-contained alkalis. Upon complete burn-off, the formation of stable bonds between the sand particles by local melting improved the mechanical resistance of the cluster in

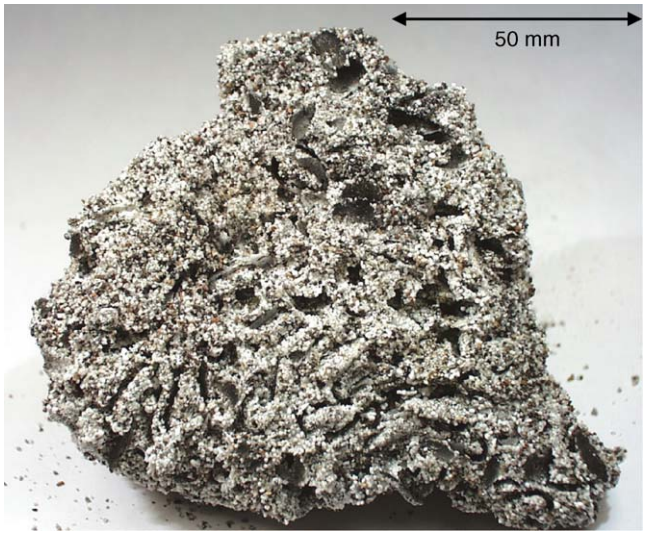


Fig. 10. Photograph of a large agglomerate from Run #12.

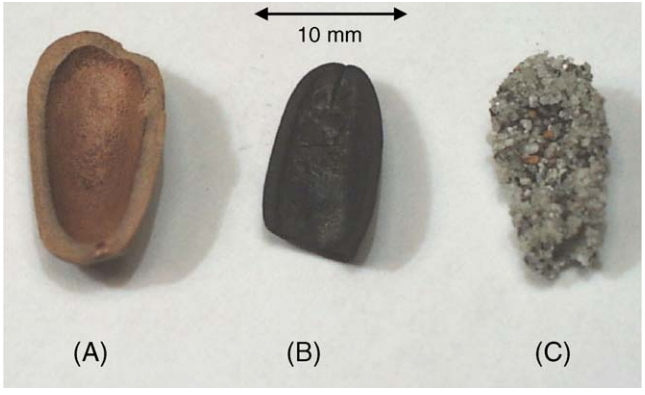


Fig. 11. Photograph of an original fuel particle (A), a char particle (B), and a small sand agglomerate (C) from Run #12.

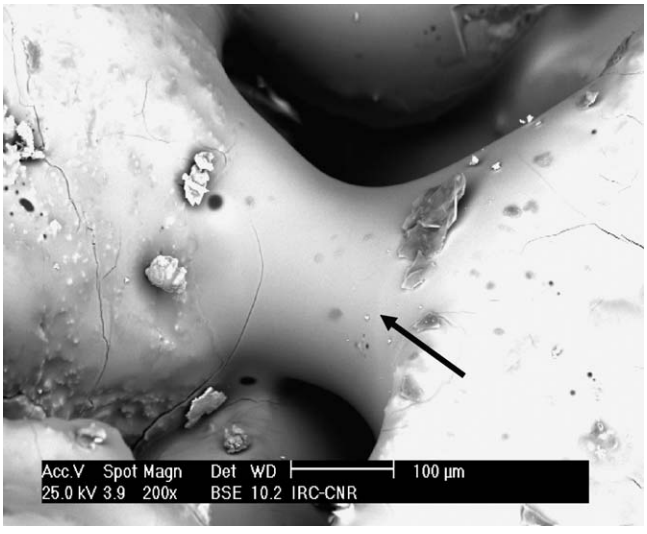


Fig. 12. SEM micrograph of the molten bridge between two sand particles in an agglomerate sample from Run #12.

spite of the low mechanical resistance of the fuel ash skeleton. The SEM micrograph reported in Fig. 12 is in line with this agglomeration mechanism; a bridge connecting two sand particles is clearly shown formed by an amorphous phase originated from molten matter, probably produced during char combustion. The bridge zone indicated by the arrow in Fig. 12 has K concentration as high as 8.5% by mass, as revealed by EDX analysis.

## 4. Conclusions

Experiments carried out in two combustors with a different scale provided further insights into the mechanism of bed agglomeration during fluidized bed combustion of a biomass fuel. In particular, among factors enhancing the tendency to bed agglomeration, the sand size, the combustor size, and the presence of internals have a prominent effect.

Two competitive processes are likely to act in the bed: the formation of stable bonds between bed particles as a consequence of low-melting point eutectic formation and the breaking of the agglomerated sand by inertial forces or impacts with internal surfaces. When the former process prevails, bed defluidization is quickly achieved, even if the formed agglomerates are relatively friable and easily breakable.

The application of a previously developed diagnostic tool for monitoring the agglomeration process was extended to a different fuel and to a larger scale. It was demonstrated that the onset of bed defluidization can be foreseen by the analysis of the pressure variance inside the bed, since the formation of small sand aggregates changes the bed size distribution and fluid dynamics. A threshold value of the variance reduction of 60–70% with respect to the initial steady state value was measured upon defluidization, irrespectively of the combustor scale and of the operating conditions.

Since the pilot facility is well representative of small industrial boilers of practical interest for biomass combustion, the diagnostic technique based on pressure variance reduction can be considered of practical interest to prevent the onset of dramatic bed defluidization events.

## Acknowledgments

A. Cammarota, A. Cante, M. Fascelli, L. Ferrante, C. Liccardi, A. Narducci and A. Silvestre are gratefully acknowledged for their assistance during combustion and agglomeration experiments. Authors are also grateful to C. Zucchini for performing the SEM-EDX analyses.

## References

[1] S.C. Saxena, C.K. Jotshi, Fluidized-bed incineration of waste materials, Prog. Energy Combust. Sci. 20 (1994) 281–324.
[2] E.J. Anthony, Fluidized bed combustion of alternative solid fuels; status, successes and problems of the technology, Prog. Energy Combust. Sci. 21 (1995) 239–268.
[3] F. Scala, P. Salatino, Modelling fluidized bed combustion of high-volatile solid fuels, Chem. Eng. Sci. 57 (2002) 1175–1196.

[4] R. Chirone, F. Miccio, F. Scala, On the relevance of axial and transversal fuel segregation during the FB combustion of a biomass, Energy Fuels 18 (2004) 1108–1117.
[5] E. Natarajan, M. Ohman, M. Gabra, A. Nordin, T. Liliedahl, A.N. Rao, Experimental determination of bed agglomeration tendencies of some common agricultural residues in fluidized bed combustion and gasification, Biomass Bioenergy 15 (1998) 163–169.
[6] B.M. Jenkins, L.L. Baxter, T.R. Miles Jr., T.R. Miles, Combustion properties of biomass, Fuel Process. Technol. 54 (1998) 17–46.
[7] B. Skrifvars, R. Backman, M. Hupa, G. Sfiris, T. Abyhammar, A. Lyngfelt, Ash behaviour in a CFB boiler during combustion of coal, peat or wood, Fuel 77 (1998) 65–70.
[8] B.D. Grubor, S.N. Oka, M.S. Ilic, D.V. Dakic, B.T. Arsic, Biomass FBC combustion-bed agglomeration problems, in: Proceedings of 13th International Conference on Fluidized Bed Combustion, 1995, pp. 515–522.
[9] J. Werther, M. Saenger, E.-U. Hartge, T. Ogada, Z. Siagi, Combustion of agricultural residues, Prog. Energy Combust. Sci. 26 (2000) 1–27.
[10] P. Salatino, F. Scala, R. Chirone, Fluidized bed combustion of a biomass char: the influence of carbon attrition and fines postcombustion on fixed carbon conversion, Proc. Combust. Inst. 27 (1998) 3103–3110.
[11] F. Scala, P. Salatino, R. Chirone, Fluidized bed combustion of a biomass char (*Robinia pseudoacacia*), Energy Fuels 14 (2000) 781–790.
[12] R. Chirone, P. Salatino, F. Scala, The relevance of the attrition to the fate of ashes during fluidized bed combustion of a biomass, Proc. Combust. Inst. 28 (2000) 2279–2286.
[13] F. Scala, R. Chirone, P. Salatino, The influence of fine char particles burnout on bed agglomeration during the fluidized bed combustion of a biomass fuel, Fuel Process. Technol. 84 (2003) 229–241.
[14] J. Latva-Somppi, E.I. Kauppinen, T. Valmari, P. Ahonen, A.S. Gurav, T.T. Kodas, B. Johanson, The ash formation during co-combustion of wood and sludge in industrial fluidized bed boilers, Fuel Process. Technol. 54 (1998) 79–94.
[15] B.-J. Skrifvars, R. Backman, M. Hupa, Characterization of the sintering tendency of ten biomass ashes in FBC conditions by a laboratory test and by phase equilibrium calculations, Fuel Process. Technol. 56 (1998) 55–67.
[16] M. Ohman, A. Nordin, B. Skrifvars, R. Backman, M. Hupa, Bed agglomeration characteristics during fluidized bed combustion of biomass fuels, Energy Fuels 14 (2000) 169–178.
[17] W. Lin, K. Dam-Johansen, Agglomeration in fluidized bed combustion of biomass—msechanisms and co-firing with coal, in: Proceedings of 15th International Conference on Fluidized Bed Combustion, 1999, pp. 1188–1191.
[18] F. Scala, R. Chirone, Characterization and early detection of bed agglomeration during the fluidized bed combustion of olive husk, Energy Fuels 20 (2006) 120–132.
[19] R.C. Brown, M.B. Dowson, J.L. Smoenk, Bed material agglomeration during fluidized bed combustion, DOE Report DOE/PC/92530, 1996.